Magnetic Targeting of Gadolinium Contrast to Enhance MRI of the Inner Ear in Endolymphatic Hydrops

Trung N. Le, MD, PhD [ID]; Wendy Oakden, PhD; Subhendu Mukherjee, PhD; Zannatul Ferdous, PhD; Maya Kuroiwa, MD [ID]; Violet M. Liu, MSc; Zhifen Zhang, PhD; Yumai Situ, MSc; Brandon Paul, PhD; Greg Stanisz, PhD

Objectives: 1. Determine the feasibility and efficiency of local magnetic targeting delivery of gadolinium (Gad) contrast to the inner ear in rodents. 2. Assess any potential ototoxicity of magnetic targeting delivery of Gad in the inner ear. 3. Study the utility of magnetic targeting delivery of Gad to visualize and quantify endolymphatic hydrops (EH) in a transgenic mouse model.

Study Design: Controlled *in vivo* animal model study.

Methods: Paramagnetic Gad was locally delivered to the inner ear using the magnetic targeting technique in both rat and mouse models. Efficiency of contrast delivery was assessed using magnetic resonance imaging (MRI). Ototoxicity of Gad was examined with histology of the cochlea and functional audiological tests. The Phex mouse model was used to study EH, hearing loss, and balance dysfunction. Magnetic targeting delivery of Gad contrast was used in the Phex mouse model to visualize the effects of EH using MRI.

Results: Magnetic targeting improved the delivery of Gad to the inner ear and the technique was reproducible in both rat and mouse models. The delivery method did not result in microstructural damage or any significant hearing loss in a normal animal. Magnetic targeting of Gad in the Phex mouse model allowed detailed visualization and quantification of EH.

Conclusion: This study provided the first evidence of the effectiveness and efficiency of the local magnetic targeting delivery of gadolinium contrast to the inner ear and its application to the visualization and quantification of EH.

Key Words: magnetic targeting, gadolinium contrast, local delivery, endolymphatic hydrops, Meniere's disease, hearing loss, MRI.

Laryngoscope, 00:1–10, 2022

INTRODUCTION

Ménière's disease (MD) is commonly referred to as endolymphatic hydrops (EH) for its pathological findings in support of increased endolymphatic pressure leading to distension and sometimes rupture of the membranous labyrinth.[1,2] Magnetic Resonance Imaging (MRI) in the presence of an exogenous gadolinium-based contrast agent (Gad) has been suggested as a potential technique to allow visualization of the cochlea. Gad accumulates in the perilymph, while the endolymphatic compartment is impermeable due to the presence of tight junctions.[3,4] In principle, EH could be visualized *in vivo* using intravenous Gad administration as is typically done in leaky tumor vasculature.[5–7] However, because of its large molecular size, Gad does not pass through the normal blood labyrinth barrier efficiently and the concentration of Gad in this compartment is typically low and takes a long time to accumulate.[8,9] High dosage intravenous administration is needed in both animal and human studies which carried the risk of systemic toxicity including nephrogenic systemic fibrosis.[10]

Local intratympanic administration of a very low dose of Gad can induce much higher concentrations of contrast in the perilymph and reduce the risk of systemic toxicity.[11,12] Our group and others have demonstrated that magnetic targeting can improve the delivery and retention of transplanted therapeutics within the inner ear both locally[13] and systemically.[14,15] Taking advantage of the paramagnetic property of gadolinium, our study demonstrates that magnetic targeting improves the local delivery of Gad to the inner ear while maintaining hearing function. Using this technique, visualization and quantification of changes to the inner ear in a transgenic animal model of EH is possible (Fig. 1).

METHODS

Animals: Animal care and handling were approved by the Committee Regulations at Sunnybrook Research Institute. Long-
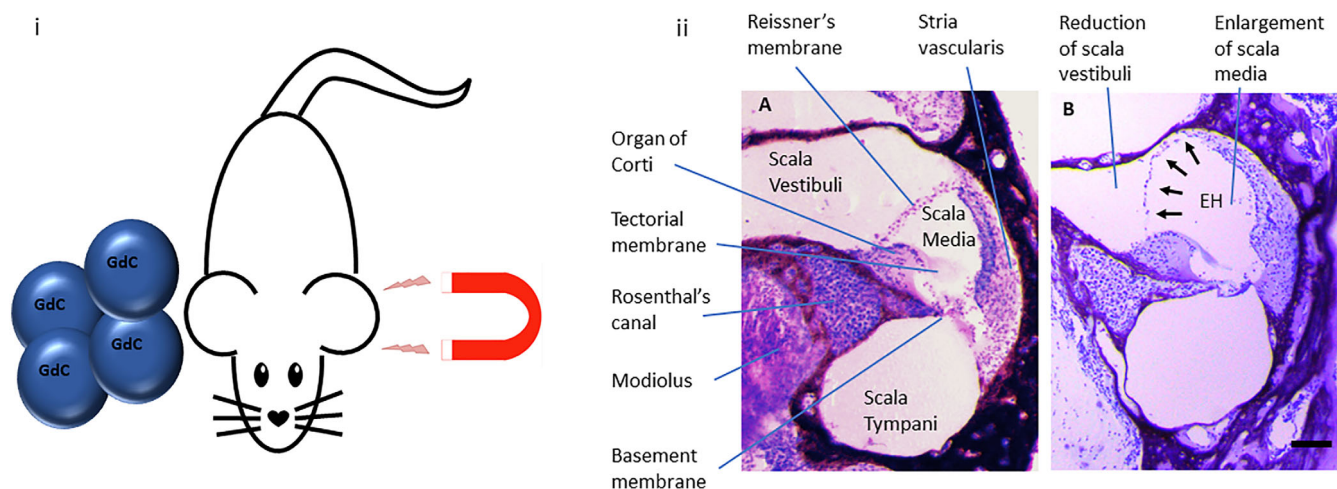
Fig. 1. (i) Schematic diagram of local magnetic targeting delivery of gadolinium contrast to the inner ear. Gad is surgically placed onto the round window (RW) membrane of an anesthetized rodent. External magnet is placed beside the contralateral ear to actively pull the contrast across the RW membrane. (ii) Cross-sections of the cochlea and the organ of Corti show the normal position of Reissner's membrane in adult control (+/Y) and distended endolymphatic space with ballooning of Reissner's membrane in PhexHyp-Duk/Y mice (black arrows). Scale bar 100 μm [Color figure can be viewed in the online issue, which is available at www.laryngoscope.com.]

Evans rats and CBA/J mice were obtained from Charles River and Jackson Laboratories. Equal numbers of male and female rats and mice were used, and the animals were 2–3 months old at the onset of the experiments (Fig. 2i). Genetic murine model of X-linked hypophosphatemia (rickets) exhibiting defects in *PhexGy* and *PhexHyp* genes served as a viable model to reproduce spontaneous, progressive hearing loss and vestibular impairment for EH.[16–18] The Phex[Hyp-Duk] mutation maintained in the BALB/c/J background was obtained from Jackson Laboratory. Male Phex[Hyp-Duk]/Y mice were used and compared to +/Y male sibling mice for all analyses. Animals were maintained at 37°C for all experiments.

Audiological function tests: Auditory Brainstem Response (ABR) and Distortion Product Otoacoustic Emission (DPOAE) were recorded using the Tucker Davis Technologies system 3 RZ6 in a free field condition with individual ears tested separately.[13,14] Animals were anesthetized with an IP injection of ketamine (100 mg/kg) and xylazine (20 mg/kg).

Round window (RW) administration of Gadolinium and magnetic targeting delivery: Animals underwent general anesthesia using 2%–3% isoflurane for the surgical intervention on the left ear (Fig. 2ii). 2–3 μl solution of 604.72 mg/ml Gadobutrol (Gadovist® 1.0, Bayer Inc., Canada) was deposited onto the RW membrane. A 0.5 Tesla magnet (K&J Magnetics, PA) was placed beside the contralateral right ear for 30 min. Right ears were untreated and used as same-animal controls.

Magnetic Resonance Imaging: MRI experiments were conducted within 30 minutes of treatment on a 7 T horizontal bore Advance BioSpec 70/30 scanner (Bruker BioSpin, Germany) using an 8 cm volume transmit coil and 20 mm receiver coil.

T1-weighted images were acquired using a 3D FLASH sequence with TE 8 ms, TR 30 ms, FA 30°, 1 average, and fat suppression. Low-resolution, 100 μm isotropic images were acquired using a $20 \times 20 \times 3.2$ mm³ FOV and 3m30s scan time, while high-resolution, 50 μm isotropic images were acquired using a $10 \times 20 \times 2.4$ mm³ FOV, and 1h3m scan time.

Gad enhancement in the cochlea was calculated using a set of regions of interest (ROIs) drawn on the horizontal cross-section of the cochlea. Corresponding ROIs were delineated in the control ears and used for signal normalization and comparison between animals.

Cochlear volume was manually delineated on each image using Aedes graphical user interface in MatLab (The MathWorks, Natick, MA) (https://github.com/mjnissi/aedes), then normalized and multiplied the signal intensities by the voxel volume in order to account for partial volume effects in MRI. Cross-sectional area of the scala media was quantified by measuring the non-enhancing region between bright scala vestibuli and scala tympani. 3D rendering was conducted using the volume rendering algorithm in 3D Slicer[19] (www.slicer.org/).

Histology: Cochleae were collected and processed for both whole-mount and cryosection.[13,14] For immunohistochemistry, Nissil staining was performed using cresyl violet acetate. For immunofluorescence, the following primary antibodies were used: (1) anti-myosin VII A (Proteus bioscience, dilution 1:1000), (2) C-terminal binding protein 2 (BD Biosciences, dilution 1:200), (3) anti-tubulin β3 (BioLegend, dilution 1:1000).[13,14] Pictures were taken with a Nikon confocal microscope with the same setting and exposure time for all images.

Forced Swim Test (FST): Recorded video was analyzed as described by Can et al.[20] Parameters of floating behavior were defined as immobility with only occasional slight movements required for keeping the body balanced and the nose above water. During the analysis, each animal's time spent mobile was measured, and the time of immobility was calculated by subtracting that number from a total of 4 min.

Balance Beam Test (BBT): Recorded video was analyzed as described by Luong et al.[21] Mice were allowed to cross the beam to get small pieces of cheese placed at the finish point. Time to cross the beam and number of slips were measured.

Statistical Analysis: Groups consisted of at least $n = 6$ animals which yields statistically powered data based on the robustness of the main endpoints to achieve 80% power at alpha of 0.05. Data were represented as mean $\pm$ SEM and analyzed in R (R Core Team, 2021). Comparisons of WT and KO groups on the FST, balance beam test, and whole-cochlea perilymph volume were made using two-samples (independent) t-tests, and Welch's t-tests in cases of unequal variances between groups as identified by Levene's test. MRI signal intensity was assessed using a 2×2 analysis of variance (ANOVA). ABR and DPOAE measurements were assessed using mixed-effects models and
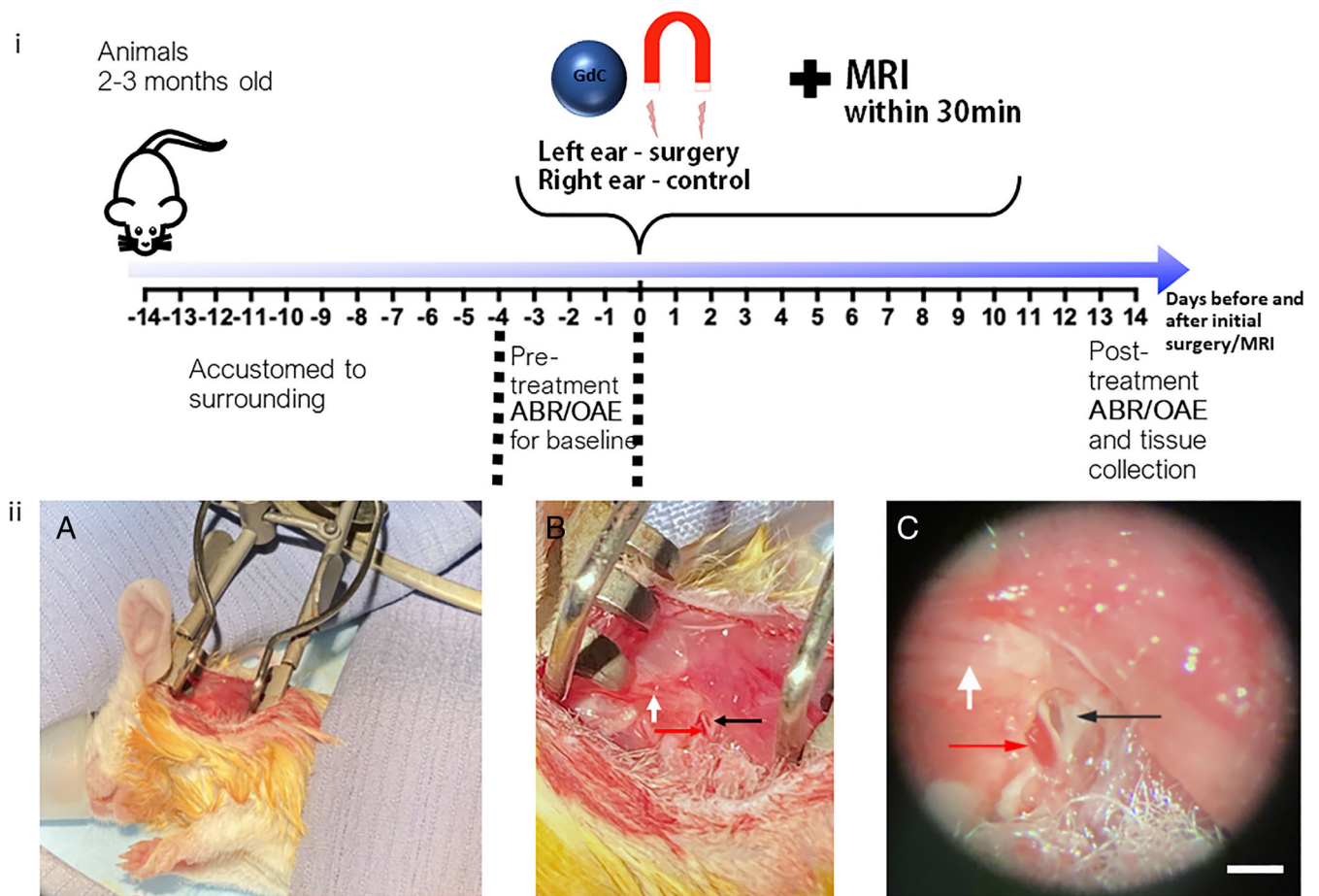
Fig. 2. (i) Experimental timeline. (ii) Surgical approach to round window niche in mice. (A) A post-auricular incision was performed to expose the tympanic bulla bone. (B) Extended drilling is necessary to remove further bulla bone and expose the round window (RW) niche. (C) Visualization of a stapedial artery (red arrow), facial nerve (white arrow), and the RW niche while maintaining the RW membrane intact (black arrow). Scale bar 100 μm [Color figure can be viewed in the online issue, which is available at www.laryngoscope.com.]

tested for significance of predictor terms using ANOVA (degrees of freedom adjusted using Satterthwaite's method). Endolymphatic area measurements were compared across animal groups and cochlear regions using the Poisson generalized linear model, with the significance of predictors assessed with likelihood ratio tests. All mixed models included animal ID as a random intercept. Post-hoc tests for all models were computed in the *emmeans* package and p values were corrected for false discovery rate. The alpha criterion for Type I error was set at 0.05.

RESULT

Efficacy of local magnetic targeting of gadolinium to the rat inner ear

MRI images in all orientations confirmed that Gad enhancement (bright signal) was observably higher in the cochlea of contrast treated ear (left ear) relative to the control untreated ear (right ear) when using either Gad alone (relying on passive diffusion), or Gad plus magnetic targeting (Fig. 3i). There was less signal enhancement with Gad alone (Fig. 3iB,D,F) in the treated left ear than with Gad plus magnetic targeting (Fig. 3iA,C,E). The effect of magnetic targeting on the MRI signal intensity

was tested in a 2×2 mixed ANOVA comparing the between-subjects factor of the group (magnetic targeting of Gad versus Gad alone) and the within-subjects factor of MRI signal enhancement over five ROIs spaced out from the basal turn to the apex (Fig. 3iiA,B). The model returned the main effect of group (F $(1, 7) = 22.94$, $p = 0.002$) indicating a higher signal intensity for the magnetic targeting of Gad compared to Gad alone. A main effect of ROI was found (F$(2.53,17.68) = 4.01$, $p = 0.029$; degrees of freedom adjusted using Greenhouse–Geisser correction, $\varepsilon = 0.63$). Post-hoc tests collapsed across the group and indicated that ROI #5 had a lower signal intensity than ROIs #1–3 (p's < 0.039), but the difference between ROI #4 and ROI #5 did not reach significance ($p = 0.06$). The interaction term between ROI and group was not significant ($p = 0.17$), suggesting that group differences in intensity were not conditioned on the cochlear ROI.

MRI results further demonstrated Gad accumulation in the cochlea, vestibule, and semicircular canals of the left ear where Gad contrast was magnetically targeted locally (Fig. 3iiiC). This three-dimensional MRI view of the inner ear showed lesser contrast enhancement of
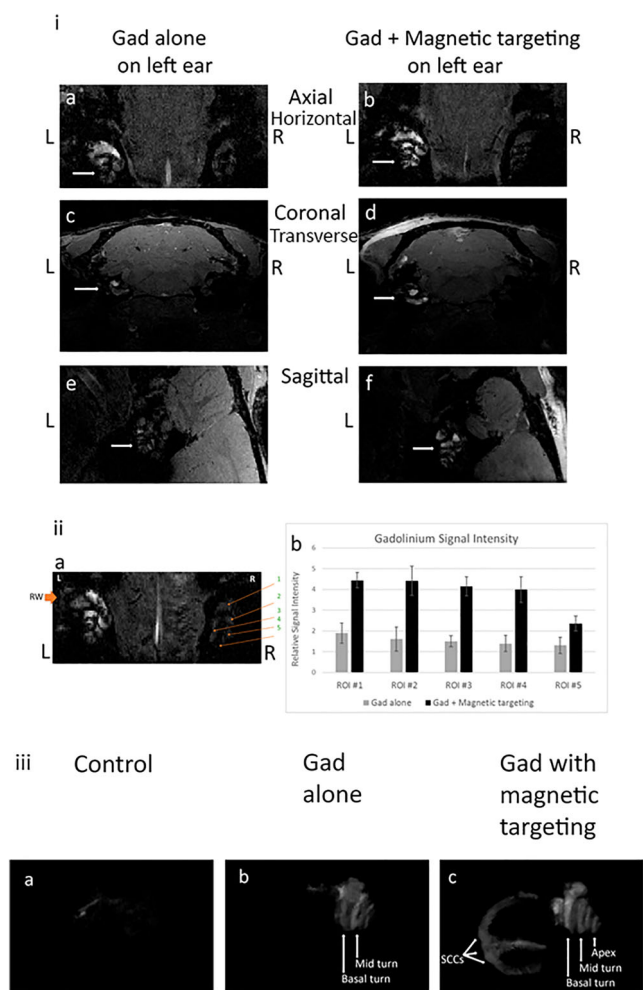
Fig. 3. Comparison of gadolinium distribution following either magnetic targeting or passive diffusion. (i) Different views (Axial or Horizontal, Coronal or Transverse, and Sagittal) of T1-weighted MRI images of rat cochleae using a 3D FLASH sequence. Left ear (L) had Gad contrast delivered surgically on top of the RW membrane while right ear (R) was kept untouched as a control. For Gad alone group, no external magnet was used (A,C,E). For the magnetic targeting group, Gad was targeted to the inner ear using an external magnet for 30 min (B,D,F). (ii) Five regions of interest (ROI) were drawn in the cochlea of both ears to compare signal intensity of Gad in both groups normalized to signal intensity in the control right ears (A). ROI #1,2 basal turn, ROI #3, 4 mid-turn, and ROI #5 apex. Grey bars represented the relative signal intensity of Gad alone, and black bars represented the relative signal intensity of Gad plus magnetic targeting (B). Bar diagrams indicate mean ± SEM values of relative MRI signal intensity. (iii) Distribution of Gad in the inner ear following magnetic targeting local delivery, visualized using 3D ImageJ. (A) Right control ear with no contrast and no magnetic targeting, (B) Left ear with surgical delivery of Gad contrast alone, (C) Left ear with surgical delivery of Gad contrast plus magnetic targeting. [Gad: gadolinium; SCCS: semicircular canals; RW: round window] [Color figure can be viewed in the online issue, which is available at www.laryngoscope.com.]

basal turn and mid-turn in Gad alone (with passive diffusion) (Fig. 3iiiB) compared to Gad plus magnetic targeting (Fig. 3iiiC). No signal enhancement was present in the control right ear (Fig. 3iiiA).

Magnetic targeting of gadolinium had no adverse effect on the inner ear hearing function

There was no significant change in ABR thresholds at any of the frequencies examined (8, 16, 24 kHz) in the treated left ear or controlled right ear up to 6 weeks after treatment in the Long Evans rat model (Fig. 4iA–D). DPOAE thresholds across high frequencies mildly increased from baseline to 6 weeks post-treatment (slope: $\beta = 26.05$, SE $= 11.54$, $p = 0.027$), but this did not differ between treated and control ears. In the CBA/J mouse model, there was a minor decrease in the ABR threshold likely due to conductive hearing loss at 2 weeks after surgery (Fig. S1). Histology of hair cells and the synaptic marker was examined in both treated and control ears for the Long Evans rat model (Fig. 4ii). The results did not show any observable loss of OHCs, IHCs, or presynaptic ribbon labeling in any of the cochlear turns (basal (>20 kHz), mid-turn (8–20 kHz), and apex (<8 kHz)) of control and or treated ears.

Similarly, for the transgenic hemizygous Phex$^{Hyp-Duk}$/Y littermates, further examination of the microstructure of the cochlea showed a comparable density of spiral ganglion neurons in Rosenthal's canal and a similar number of OHCs and IHCs in Organ of Corti (Fig. S2C–F) between genotypes after magnetic targeting of Gad. The neuronal degenerative difference was in the density of central neuronal processes within the modiolus with higher density found in wild-type compared to mutant littermates (Fig. S2G,H, arrows).

Phex mouse model exhibits rapid progressive hearing loss at P120

Auditory results showed that the hearing loss can be rapid and progressive to a severe-profound level for knockout mutants at P120 (Fig. 5i,ii). This was confirmed in the statistical model thresholds, with a significant interaction of group and time point of testing (ABR: $F(3,150) = 5.26$, $p = 0.0018$; OAE: $F(3,150) = 7.76$, $p < 0.001$) and group and test frequency (ABR: $F(9,150) = 3.39$, $p = 0.0008$; OAE: $F(9,150) = 2.90$, $p = 0.003$). Post-hoc tests found elevated ABR thresholds pre-surgery at all test frequencies in the KO group, and for 16 and 24 kHz post-surgery (p's < 0.039). OAE thresholds were elevated in the KO group pre-surgery at 16 and 24 kHz in both ears, and at 8 kHz in the right ear and 32 kHz in the left ear (p's < 0.028). Post-surgery thresholds in the KO group were elevated for both ears only at 24 kHz (p's = 0.0281). Averaged across frequencies, post-surgery ABR thresholds were elevated in both KO ($p = 0.034$) and WT ($p < 0.001$) groups in the left ear compared to pre-surgery. For OAE, thresholds only elevated post-surgery for the WT group ($p < 0.0001$). It was noteworthy however in ABR wave I amplitude between genotypes with KO showed deterioration across all frequencies measured at 8, 16, 24, and 32 kHz (Fig. 5iiA–D vs. E–H). The hearing loss in KO was in the severe-profound range at this time wave I amplitude could not be reliably measured due to poor signal-to-noise ratio and no statistical calculation was possible.
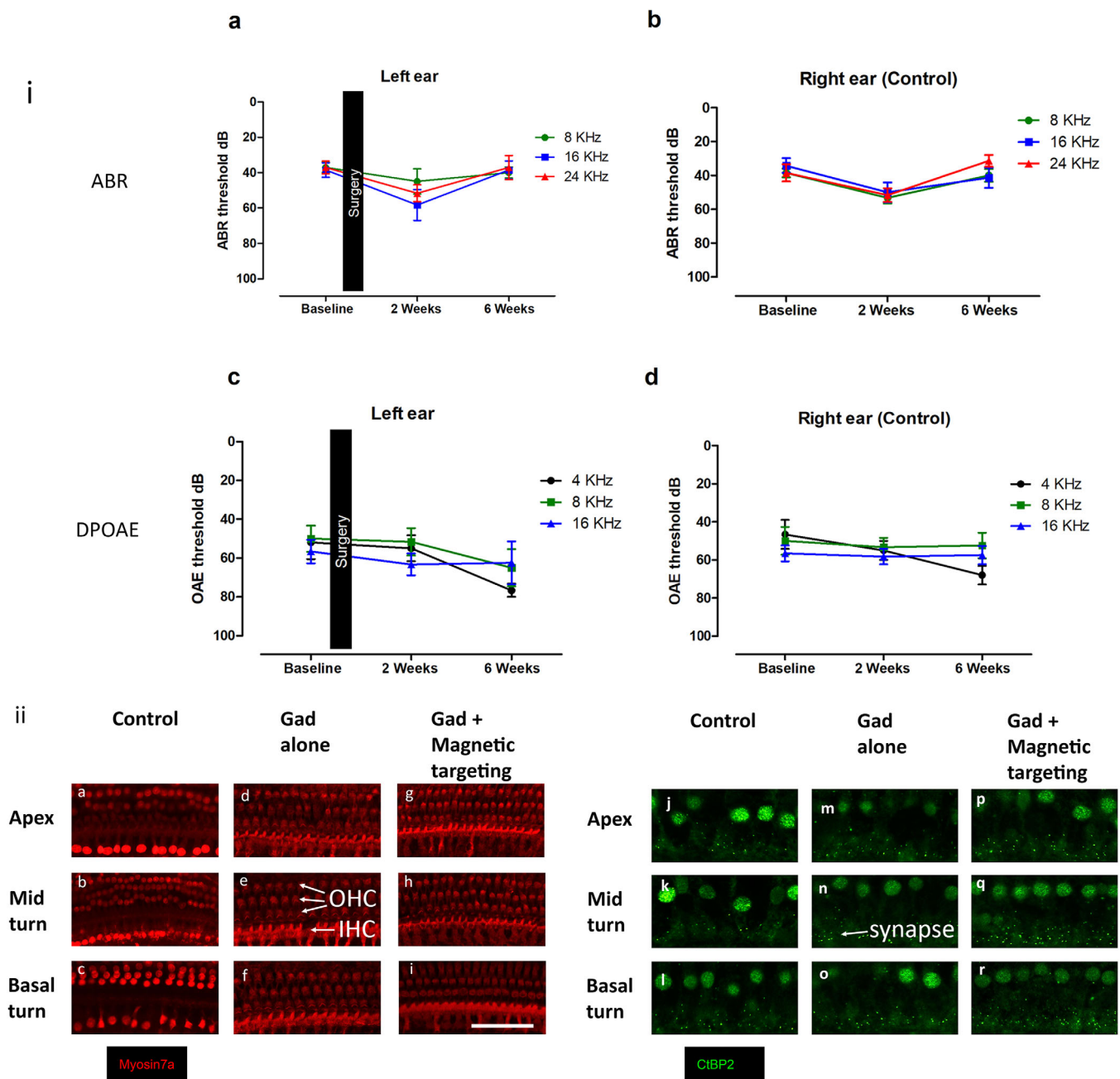
Fig. 4. Magnetic targeting of gadolinium had no observable adverse effect on hearing and cellular microstructures in the inner ear of the Long Evans rat model. (i) Average of ABR and DPOAE thresholds in Gad plus magnetic targeting treated left ear (A,C) compared to control right ear (B,D) at 8, 16, 24 kHz before and after 2 and 6 weeks of magnetic targeting delivery of Gad contrast. The black vertical bar (A,C) indicated the time of Gad administration. Mean ± SEM values of the ABR threshold are shown in the graphs for n = 6–7 animals. (ii) Immunostaining of cochlear hair cells (anti-Myosin VIIa, red stain) and presynaptic ribbons (anti-ctBP2, green stain) in the whole-mount organ of Corti of control, Gad alone, and Gad plus magnetic targeting ears. White arrows indicate outer hair cells (OHCs), inner hair cells (IHCs), and synapses. Scale bar 50 μm [Color figure can be viewed in the online issue, which is available at www.laryngoscope.com.]

Phex mouse model exhibits objective vestibular dysfunction

For the BBT, both WT and KO littermates were allowed to cross the beam to find the cheese (Fig. 6iA,B and Video S1 in Appendix S1). The WT took an average of 12.7 ± 2.3 s to cross the beam while the KO took an average of 28.8 ± 5.4 s (two-samples $t(10) = 3.05$, $p = 0.0123$). The WT also had an average of less than one slip while the KO had an average of 3.9 ± 0.3 slips (Welch's $t(11.6) = 4.77$, $p = 0.0001$). For FST, the time of activity was measured during the final 4-min period (Fig. 6ii and Video S2 in Appendix S1). The WT was able to float and became immobile with only occasional slight movements required for keeping the body balanced and the nose above water. The average immobility time for WT is 141.3 ± 13.7 s compared to 43.9 ± 14.3 seconds of
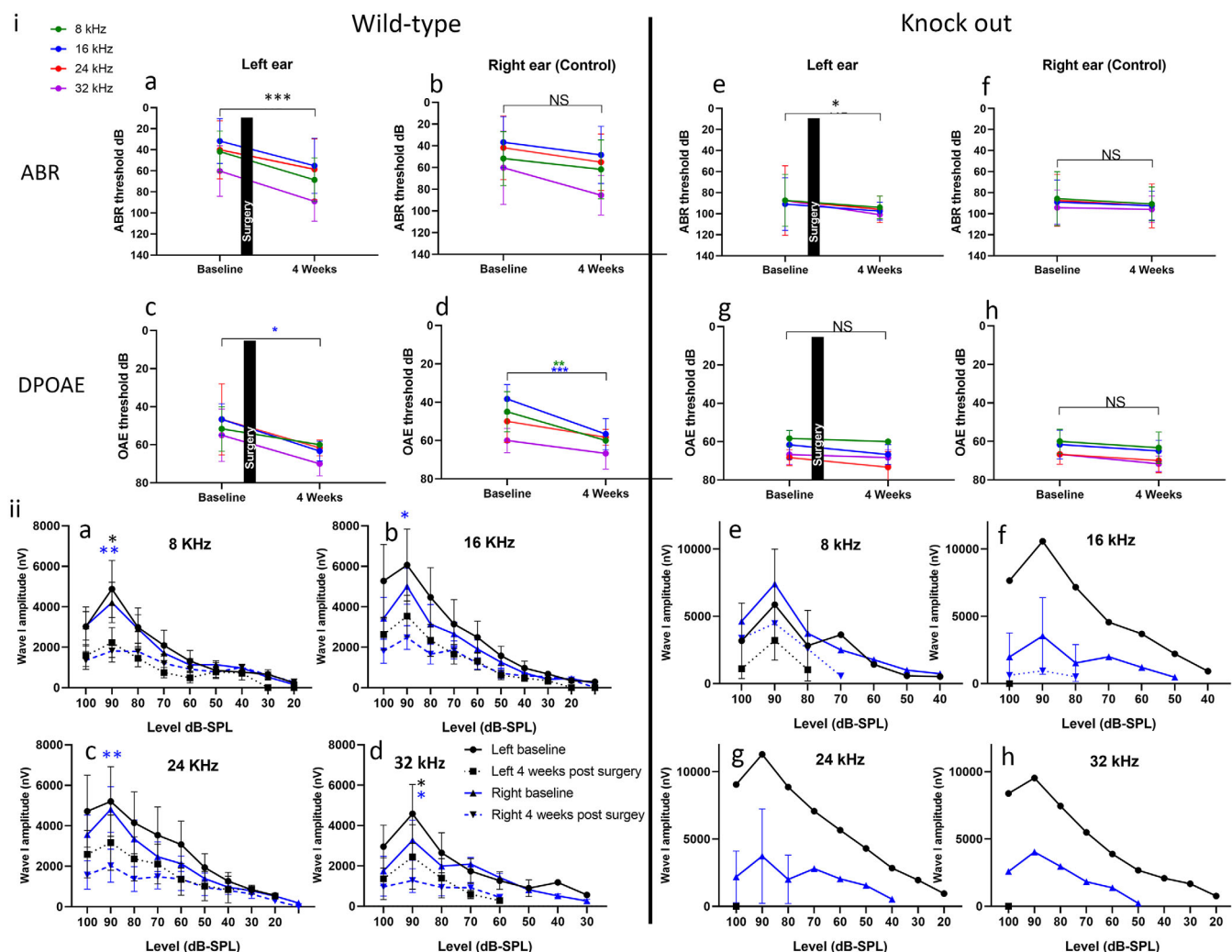
Fig. 5. Audiological examination of Phex mouse at P120 age within 4 weeks of magnetic targeting, surgery, and MRI treatment of the left ear. (i) ABR and DPOAE absolute thresholds were measured in both ears of wild-type (A–D) and knockout (E–H) mutant littermates. ii) ABR wave I amplitudes were measured by evoking at suprathreshold tones in both ears of wild-type (a-d) and knockout mutant (E–H) littermates, respectively, at different frequencies (8, 16, 24, 32 kHz). There was no measurable postoperative wave I amplitude in the knockout littermates due to severe-profound hearing loss at this age. Graphs represented mean ± SEM values of the threshold or amplitude values. ABR amplitudes above 65 dB SPL (i.e., averaged across stimulus levels) were attenuated in the WT group when averaged across all frequencies. $*p < 0.05$, $**p < 0.01$, $***p < 0.001$, NS = no significance, $n = 6$ animals [Color figure can be viewed in the online issue, which is available at www.laryngoscope.com.]

KO (two-sample t(18) = 4.86) (Fig. 6iiiC,D). The KO continued to be active, constantly moving both hind legs and tail to maintain balance and keep the nose above water. The average mobility time for KO is 196.1 ± 14.3 s compared to 98.7 ± 13.7 s of WT (two-sample t(18) = 4.86, $p = 0.0001$).

Magnetic targeting enhanced gadolinium local delivery to the inner ear and captured EH effectively in the Phex mouse

The left treated cochlea was brightly enhanced with Gad (Fig. 7i) compared to no enhancement of the right control ear (Figs. 3iiA,iiiA and 7iiiA). Furthermore, perilymphatic compartments, such as scala tympani and scala vestibuli, were brightly labeled and allowed

visualization of dark scala media in the middle (Fig. 7i, arrows). There was a clear difference between the size of the endolymphatic compartment (scala media) with a small and narrow area in WT compared to a larger and wider area with a circular shape in KO littermates (Fig. 7i,ii). Average cross-sectional area measurements of endolymphatic space in both basal and mid turns were significantly smaller in WT (+/Y) than in KO (Phex$^{Hyp-Duk}$/Y) (main effect of group, $X^2(1) = 12.70$, $p = 0.0003$) (Fig. 7iiiB). Post-hoc tests indicated that the difference was significant for all tested cochlear locations (p's < 0.0001).

Volumetric 3D images for the entire cochlea demonstrated a larger endolymphatic compartment (without contrast) in the KO compared to WT littermates (Fig. 8i). In WT, scala tympani and scala vestibuli were filled with
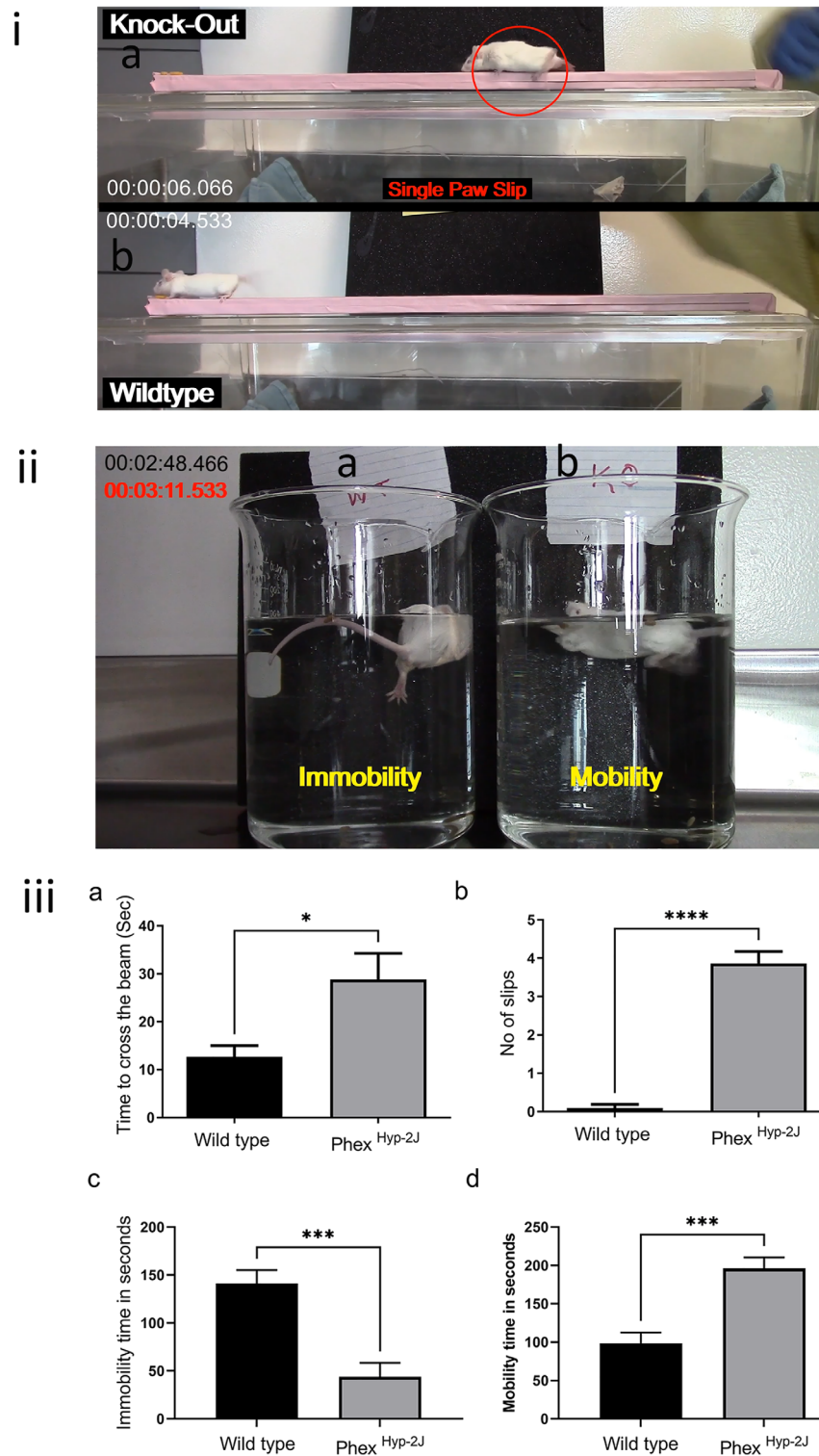
Fig. 6. Balance tests of Phex mouse at P120 age. (i) Balance beam test for both wild-type (B) and mutant (A) littermates with measurement of time to cross the beam and number of slips. Corresponding to Video S1 in Appendix S1. (ii) Forced swim test for both wild-type (a) and mutant (b) littermates with measurement of time of immobility and mobility during the final 4 minutes of the test. Corresponding to Video S1 in Appendix S1. (iii) Graphs represented mean ± SEM values of time to cross the beam (A) and the number of slips (B), time spent immobile (C), and time spent mobile (D). *$p < 0.05$, ***$p < 0.001$, ****$p < 0.0001$, $n = 6$ animals. Note that one mouse could not fully complete the task in the knockout group. [Color figure can be viewed in the online issue, which is available at www.laryngoscope.com.]
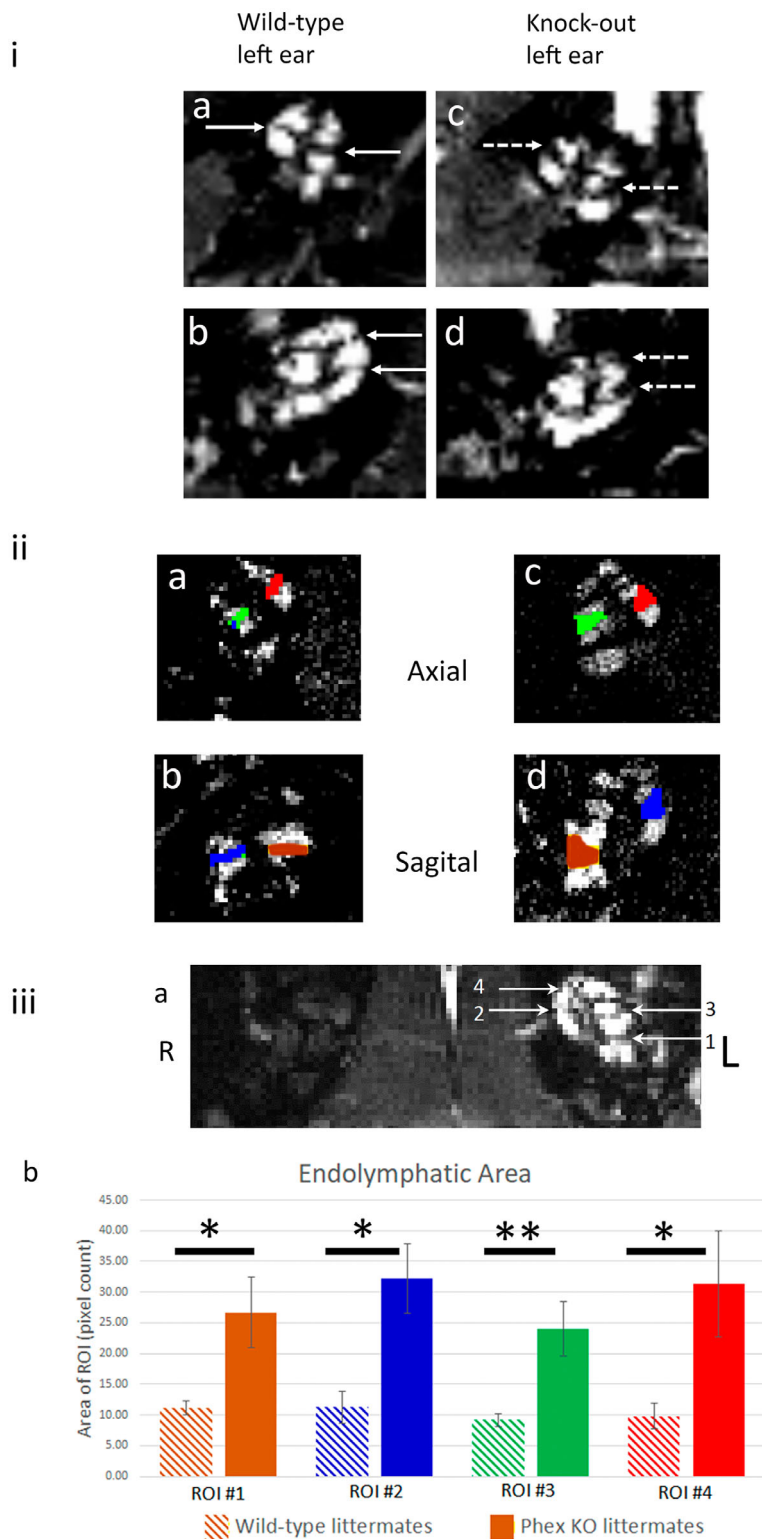
Fig. 7. Estimation of the endolymphatic cross-sectional area following Gad plus magnetic targeting in Phex mouse and wild-type using two orthogonal planes. (i) Left ears of wild-type (A,B) and mutant (C,D) littermates with Gad contrast in the perilymphatic compartments (bright signal in scala tympani and scala vestibuli) leaving non-enhanced endolymphatic compartment (scala media appeared dark). Scala media was indicated by solid arrows for wild-type and dashed arrows for the knockout. Axial (A,C) and sagittal (B,D) views. (ii) ROIs were drawn in the endolymphatic compartment (scala media) using Aedes in MatLab (red and green for the mid-turn, blue and yellow for the basal turn) in axial (A,C) and sagittal (B,D) views. (iiia) Different endolymphatic compartments of basal turn (1 and 2) and mid-turn (3 and 4) were measured and plotted to compare wild-type and knockout left ear (L). (iiib) Graphs represented mean ± SEM values of the area of the endolymphatic compartment or scala media (solid bar for wild-type, dash bar for mutant). *$p < 0.05$, **$p < 0.01$, $n = 6$ animals [Color figure can be viewed in the online issue, which is available at www.laryngoscope.com.]
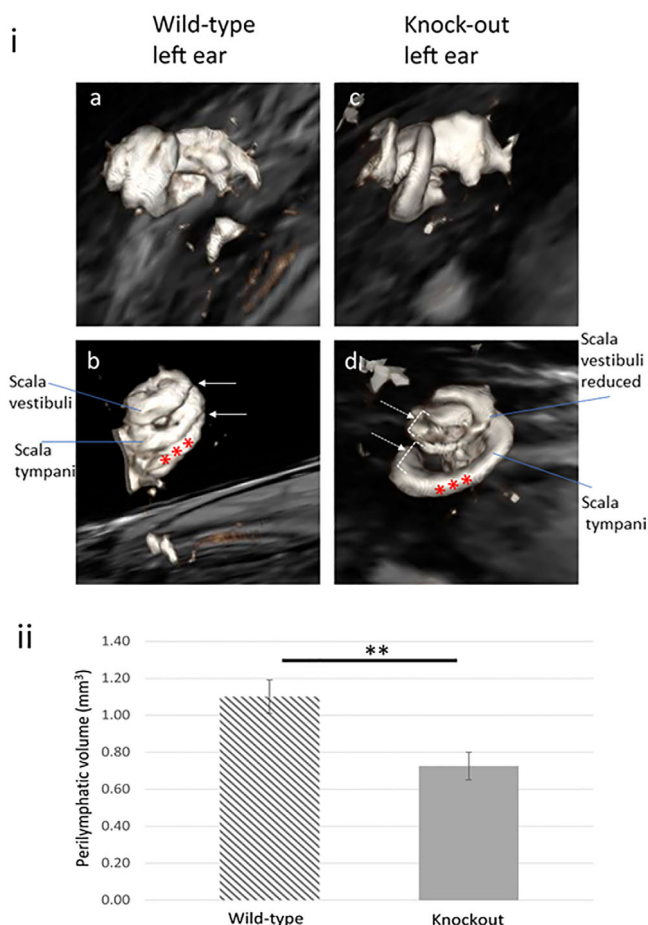
Wild-type
left ear

Knock-out
left ear

Fig. 8. 3D rendering of endolymphatic hydrops of Phex mouse model after magnetic targeting of gadolinium and MRI. (i) Left ears of wild-type (A,B) and mutant (C,D) littermates were enhanced with Gad contrast in perilymphatic compartments (bright scala tympani and scala vestibuli) leaving non-enhanced endolymphatic compartment (dark scala media - the contrast-free space between two bright compartments). Solid arrows for scala media of wild-type, dashed arrows for scala media of knockout at basal turn and mid-turn. Scala media was significantly enlarged in knockout compared to wild-type and compressed the adjacent scala vestibuli. (ii) Volumetric measurements of bright contrast signal in peri-lymphatic spaces (scala tympani and scala vestibuli, red stars) of the entire cochlea were rendered and plotted to compare between wild-type and knockout. Graphs represented mean $\pm$ SEM values of volume of perilymphatic spaces. **$p < 0.01$, $n = 6$ animals. Gad contrast was also seen in the vestibule (A,C), however, this signal was not factored into the volumetric measurement as it was outside of cochlea. [Color figure can be viewed in the online issue, which is available at www.laryngoscope.com.]

contrast (bright) as they flanked the narrow, slit-like scala media (Fig. 8iA,B). In KO mice, the scala tympani remained relatively unchanged in size, while the scala vestibuli was significantly reduced in size and largely replaced by the enlargement of the scala media or EH (Fig. 8iC,D). The scala vestibuli was so compressed that the rendering only showed the scala tympani of the subsequent turn (Fig. 8iC,D). This 3D rendering also allowed volumetric measurement of contrast-filled perilymphatic spaces (scala tympani + scala vestibuli) of the entire cochlea showing significantly smaller perilymphatic

volume in the KO compared to WT littermates (two-samples t(13) = −3.22, $p = 0.006$) (Fig. 8ii).

DISCUSSION

Direct histopathological identification of endolymphatic hydrops (EH) is the only method to unambiguously diagnose Meniere's disease (MD) while limited only to post-mortem studies. The ability to visualize cochlear changes attributable to EH by MRI is now clinically feasible, and it is likely to evolve into an important objective measure with each iteration of technical advancement. MRI scanners with 7 Tesla magnetic fields are now approved for clinical use and will provide the even greater resolution required for imaging very fine structures such as the inner ear.[22,23]

Several research groups have demonstrated that inner ear compartments can be distinguished using gadolinium-enhanced MRI.[2,4,7,24–29] Both animal and human studies utilized either systemic intravenous or local intratympanic route of contrast delivery, yet an efficient and effective delivery technique to the inner ear is not yet established. Intratympanic administration of gadolinium provides local loading of contrast agent in the vicinity of inner ear perilymph and reduced the risk for systemic toxicity. This approach however requires the ability of the contrast to diffuse through the RW membrane or oval window annular ligament[30,31] mainly based on size, polarity, and duration of contact with the membrane.[11] The majority of the contrast gets lost by clearance through the eustachian tube. Additionally, this approach does not guarantee effective distribution of the contrast along the cochlea due to the low flow rate of perilymph within the cochlea. Hence, image quality can be compromised as a result of impaired Gad accumulation when using only passive diffusion. In this study, we took advantage of the paramagnetic properties of gadolinium in conjunction with magnetic targeting to improve the accumulation of Gad in the inner ear (Fig. 3).

In agreement with the literature, we did not observe any significant loss of hearing, inner- or outer hair cells, or presynaptic ribbons following magnetic targeting of Gad in both rats and mice (Fig. 4). Gad is generally safe *in vivo* with a half-life of approximately 1.5 h, and more than 90% is excreted by the kidney within 24 h.[32] Available published data showed no adverse effects over the short and long term in healthy ears of both animals and human.[33] Further vestibular testing should be considered to fully assess gadolinium safety in the inner ear.

Several guinea pig models have been developed to mimic EH but their consistency and relevance to the study of MD are debatable.[34] The transgenic Phex model exhibits spontaneous, postnatal, progressive EH which recapitulates many aspects of clinical MD in human[16] but is only available as a mouse model (Fig. 1ii). Our study used 3-month-old mice to capture the loss of spiral ganglion neurons without hair cell loss (Fig. S2 and Fig. 5) in agreement with literature[16]; although further study is needed for the pathophysiology of asymmetrical and profound hearing loss in this model. Objective balance beam and forced swim tests of the Phex mouse demonstrated

reproducible and significant balance dysfunction (Fig. 6, Video S1 and S2). Both tests are relatively short, low-cost, require no training of the mice, and can be conducted with minimal equipment.

Our study is the first to show the effectiveness and efficiency of the local magnetic targeting delivery of Gad to the inner ear of a Phex mouse, and to provide quantification of EH in both 2D areas (Fig. 7) and 3D volumetric parameters (Fig. 8). Previous studies detected EH in guinea pigs which was a larger model but still resulted in lesser resolution than our results despite using equivalent MRI strength.[4,29] The use of magnetic targeting to enhance Gad contrast delivery to the inner ear opens up the possibility of improving and standardizing a clinical MRI method for diagnosing EH in patients.

CONCLUSION

Gadolinium is a safe and useful contrast to visualize the inner ear without local ototoxicity. Magnetic targeting can significantly enhance gadolinium delivery to the inner ear and potentially can be applied to other biological drug therapies for clinical treatments of a wide range of inner ear aetiologies.

CONFLICT OF INTEREST

The authors have no funding, financial relationships, or conflicts of interest to disclose.

BIBLIOGRAPHY

1. Merchant SN, Adams JC, Nadol JB Jr. Pathophysiology of Meniere's syndrome: are symptoms caused by endolymphatic hydrops? *Otology & Neurotology: Official Publication of the American Otological Society, American Neurotology Society [and] European Academy of Otology and Neurotology*. 2005;26:74-81.
2. Gürkov R, Flatz W, Louza J, Strupp M, Krause E. In vivo visualization of endolyphatic hydrops in patients with Meniere's disease: correlation with audiovestibular function. *European archives of Oto-Rhino-Laryngology: Official Journal of the European Federation of Oto-Rhino-Laryngological Societies (EUFOS): affiliated with the German Society for Oto-Rhino-Laryngology - Head and Neck Surgery*. 2011;268:1743-1748.
3. Lingam RK, Connor SEJ, Casselman JW, Beale T. MRI in otology: applications in cholesteatoma and Ménière's disease. *Clin Radiol*. 2018;73:35-44.
4. Niyazov DM, Andrews JC, Strelioff D, Sinha S, Lufkin R. Diagnosis of endolymphatic hydrops in vivo with magnetic resonance imaging. *Otology & Neurotology: Official Publication of the American Otological Society, American Neurotology Society [and] European Academy of Otology and Neurotology*. 2001;22:813-817.
5. Zou J, Pyykkö I, Bjelke B, Dastidar P, Toppila E. Communication between the perilymphatic scalae and spiral ligament visualized by in vivo MRI. *Audiol Neurootol*. 2005;10:145-152.
6. Naganawa S, Sugiura M, Kawamura M, Fukatsu H, Sone M, Nakashima T. Imaging of endolymphatic and perilymphatic fluid at 3T after intratympanic administration of gadolinium-diethylene-triamine pentaacetic acid. *AJNR Am J Neuroradiol*. 2008;29:724-726.
7. Naganawa S, Nakashima T. Visualization of endolymphatic hydrops with MR imaging in patients with Ménière's disease and related pathologies: current status of its methods and clinical significance. *Jpn J Radiol*. 2014;32:191-204.
8. Le TN, Blakley BW. Mannitol and the blood-labyrinth barrier. *Journal of Otolaryngology - head & neck surgery = Le Journal d'oto-rhino-laryngologie et de chirurgie cervico-faciale*. 2017;46:66.
9. Zou J, Zhang W, Poe D, Zhang Y, Ramadan UA, Pyykkö I. Differential passage of gadolinium through the mouse inner ear barriers evaluated with 4.7T MRI. *Hear Res*. 2010;259:36-43.
10. Thomsen HS. Gadolinium-based contrast media may be nephrotoxic even at approved doses. *Eur Radiol*. 2004;14:1654-1656.
11. Yoshioka M, Naganawa S, Sone M, Nakata S, Teranishi M, Nakashima T. Individual differences in the permeability of the round window: evaluating the movement of intratympanic gadolinium into the inner ear. *Otology & Neurotology: Official Publication of the American Otological Society, American Neurotology Society [and] European Academy of Otology and Neurotology*. 2009;30:645-648.
12. Plontke SK, Salt AN. Local drug delivery to the inner ear: principles, practice, and future challenges. *Hear Res*. 2018;368:1-2.
13. Mukherjee S, Kuroiwa M, Oakden W, et al. Local magnetic delivery of adeno-associated virus AAV2(quad Y-F)-mediated BDNF gene therapy restores hearing after noise injury. *Molecular Therapy: The Journal of the American Society of Gene Therapy*. 2022;30:519-533.
14. Le TN, Straatman L, Yanai A, et al. Magnetic stem cell targeting to the inner ear. *Journal of Magnetism and Magnetic Materials*. 2017;443:385-396.
15. Ramaswamy B, Roy S, Apolo AB, Shapiro B, Depireux DA. Magnetic nanoparticle mediated steroid delivery mitigates cisplatin induced hearing loss. *Front Cell Neurosci*. 2017;11:268.
16. Megerian CA, Semaan MT, Aftab S, et al. A mouse model with postnatal endolymphatic hydrops and hearing loss. *Hear Res*. 2008;237:90-105.
17. Sheykholeslami K, Megerian CA, Zheng QY. Vestibular evoked myogenic potentials in normal mice and Phex mice with spontaneous endolymphatic hydrops. *Otology & Neurotology: Official publication of the American Otological Society, American Neurotology Society [and] European Academy of Otology and Neurotology*. 2009;30:535-544.
18. Lorenz-Depiereux B, Guido VE, Johnson KR, et al. New intragenic deletions in the Phex gene clarify X-linked hypophosphatemia-related abnormalities in mice. *Mammalian Genome: Official Journal of the International Mammalian Genome Society*. 2004;15:151-161.
19. Fedorov A, Beichel R, Kalpathy-Cramer J, et al. 3D slicer as an image computing platform for the quantitative imaging network. *Magn Reson Imaging*. 2012;30:1323-1341.
20. Can A, Dao DT, Arad M, Terrillion CE, Piantadosi SC, Gould TD. The mouse forced swim test. *Journal of Visualized Experiments*. 2012;59:e3638.
21. Luong TN, Carlisle HJ, Southwell A, Patterson PH. Assessment of motor balance and coordination in mice using the balance beam. *Journal of Visualized Experiments*. 2011;49:2376.
22. Nowogrodzki A. The world's strongest MRI machines are pushing human imaging to new limits. *Nature*. 2018;563:24-26.
23. Schaefer DJ, Bourland JD, Nyenhuis JA. Review of patient safety in time-varying gradient fields. *Journal of Magnetic Resonance Imaging*. 2000;12:20-29.
24. Attyé A, Eliezer M, Medici M, et al. In vivo imaging of saccular hydrops in humans reflects sensorineural hearing loss rather than Meniere's disease symptoms. *Eur Radiol*. 2018;28:2916-2922.
25. Ikeda M, Sando I. Endolymphatic duct and sac in patients with Meniere's disease. A temporal bone histopathological study. *Ann Otol Rhinol Laryngol*. 1984;93:540-546.
26. Ito T, Inui H, Miyasaka T, et al. Three-dimensional magnetic resonance imaging reveals the relationship between the control of vertigo and decreases in endolymphatic hydrops after endolymphatic sac drainage with steroids for Meniere's disease. *Front Neurol*. 2019;10:46.
27. Lopez-Escamez JA, Attyé A. Systematic review of magnetic resonance imaging for diagnosis of Meniere disease. *Journal of Vestibular Research: Equilibrium & Orientation*. 2019;29:121-129.
28. Zou J, Poe D, Bjelke B, Pyykko I. Visualization of inner ear disorders with MRI in vivo: from animal models to human application. *Acta Otolaryngol Suppl*. 2009;129:22-31.
29. Zou J, Pyykkö I, Bretlau P, Klason T, Bjelke B. In vivo visualization of endolymphatic hydrops in Guinea pigs: magnetic resonance imaging evaluation at 4.7 tesla. *Ann Otol Rhinol Laryngol*. 2003;112:1059-1065.
30. King EB, Salt AN, Eastwood HT, O'Leary SJ. Direct entry of gadolinium into the vestibule following intratympanic applications in Guinea pigs and the influence of cochlear implantation. *Journal of the Association for Research in Otolaryngology*. 2011;12:741-751.
31. Salt AN, Hirose K. Communication pathways to and from the inner ear and their contributions to drug delivery. *Hear Res*. 2018;362:25-37.
32. Malikova H, Holesta M. Gadolinium contrast agents - are they really safe? *J Vasc Access*. 2017;18:1-7.
33. Louza J, Krause E, Gürkov R. Hearing function after intratympanic application of gadolinium-based contrast agent: a long-term evaluation. *Laryngoscope*. 2015;125:2366-2370.
34. Nakashima T, Pyykkö I, Arroll MA, et al. Meniere's disease. *Nature Reviews Disease Primers*. 2016;2:16028.